The MICADO first light imager for the ELT: SCAO LQG control performance with windshake, vibrations and mirror dynamics

Amal Zidi, Henri-François Raynaud, Caroline Kulcsár, Fabrice Vidal, Éric Gendron, Yann Clénet, Richard Davies

The MICADO first light imager for the ELT: SCAO LQG control performance with windshake, vibrations, and mirror dynamics

Amal Zidi, Henri-François Raynaud, Caroline Kulcsár, Fabrice Vidal, Eric Gendron, et al.

Amal Zidi, Henri-François Raynaud, Caroline Kulcsár, Fabrice Vidal, Eric Gendron, Yann Clénet, Richard Davies, "The MICADO first light imager for the ELT: SCAO LQG control performance with windshake, vibrations, and mirror dynamics," Proc. SPIE 12185, Adaptive Optics Systems VIII, 121852P (29 August 2022); doi: 10.1117/12.2629863

SPIE.

Event: SPIE Astronomical Telescopes + Instrumentation, 2022, Montréal, Québec, Canada

The MICADO first light imager for the ELT: SCAO LQG control performance with windshake, vibrations and mirror dynamics

Amal Zidi[a,b], Henri-François Raynaud[b], Caroline Kulcsár[b], Fabrice Vidal[a], Eric Gendron[a], Yann Clénet[a], and Richard Davies[c]

[a]LESIA, Observatoire de Paris, Université PSL, CNRS, Sorbonne Université, Université de Paris Cité
[b]LCF, IOGS, CNRS, Université Paris Saclay
[c]Max-Planck-Institut für Extraterrestrische Physik

ABSTRACT

MICADO (Multi-AO Imaging Camera for Deep Observations), the ELT first-light imager, will face the impact of windshake and vibrations, especially on tip and tilt modes. Standard integral control fails to reach MICADO-SCAO targeted performance. The presented data-driven predictive tip-tilt controller accounts for the variability of observational conditions and is shown to efficiently manage this windshake and vibration issue. We show how the impact of M4 temporal dynamics can be simulated without increasing the simulation sampling period and we assess performance with these dynamics for both regulators.

Keywords: ELT, SCAO, MICADO, windshake, vibrations, mirror dynamics

1. INTRODUCTION

The Extremely Large Telescope (ELT) is defined to be the new giant and largest telescope in the world featuring a primary mirror of 39m diameter. It will observe in near-infrared using 5 instruments among them MICADO. The selected first light instrument MICADO[1] is a near-infrared imager (0.8-2.4µm) using two adaptive optics modules. The first module is a Single Conjugate Adaptive Optics (SCAO) offered at first light, in late 2027, and developed within the MICADO consortium.[2] The second module is Multi-Conjugate Adaptive Optics (MCAO) developed by the MORFEO consortium[3] and offered few years later after SCAO. MICADO AO will drive two correction mirrors: ELT M4, a deformable mirror with fast response and small amplitudes of strokes, and ELT M5, with slow dynamics and large tip-tilt strokes.

In this article, we focus on MICADO-SCAO module. We show how to build an efficient control for MICADO-SCAO in different observations conditions including wind induced disturbances and mechanical vibrations. We propose a model-data-based Linear Quadratic Gaussian (LQG) tip/tilt controller and compare its performance to standard integrator. Finally, we evaluate the impact of M4's temporal dynamics on AO performance and propose ways to mitigate it.

2. MICADO SCAO SYSTEM

The MICADO SCAO system is making use of two correction mirrors:

- ELT M4, a deformable mirror composed of 6 petals, with around 5 000 actuators.
- ELT M5, a tip-tilt plane mirror having exactly 2 actuators.

Corresponding author: Amal Zidi, e-mail: amal.zidi@obspm.fr

Adaptive Optics Systems VIII, edited by Laura Schreiber, Dirk Schmidt, Elise Vernet,
Proc. of SPIE Vol. 12185, 121852P · © 2022 SPIE
0277-786X · doi: 10.1117/12.2629863

The SCAO system also features a pyramid wavefront sensor (WFS) delivering around 27 000 measurements.

MICADO SCAO will be exposed to windshake and vibrations. This requires to develop a high-performance control in order to bring the error budget within the targeted performance. This target is given in Strehl ratio at the wavelength of 2.2µm (K-band). It must not be far from 70% at high flux and for median seeing conditions.

3. SCENARIOS

In this article, we will consider following three scenarios:

1. [**ATM**]: atmospheric turbulence given by an ESO median profile, with Fried parameter $r_0 = 14.4$ cm;

2. [**ATM**]+[**WIND**]: in this scenario, we use the same turbulence sequences as in scenario 1 and we add to them a sequence of windshake provided by ESO and generated by a finite element model for the worst observations conditions of the telescope;

3. [**ATM**]+[**WIND**]+[**VIB**]: we add to scenario 2 a sequence of vibrations generated by a second order stochastic model, with 3 vibration peaks spread over a large frequency range: 20 Hz, 60 Hz and 200 Hz, with a total amplitude of 42 mas rms.

4. ADAPTIVE OPTICS LOOP

We consider the classical AO block diagram in Fig. 1, where ϕ^{tur}, ϕ^{cor}, ϕ^{res}, u and y are given in a modal basis and represent respectively the turbulent, correction and residual phases, the controls and the noisy measurements. (This implies that all these vectors have the same length, namely the number of controlled modes.)

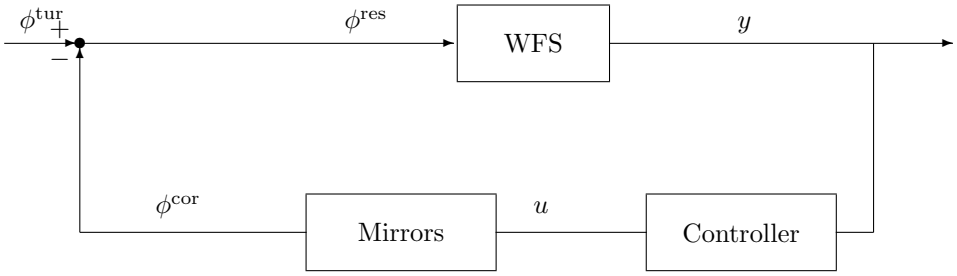

Figure 1. Block diagram of AO loop

5. TESTED CONTROLLERS FOR END-TO-END SIMULATIONS

Because windshake and vibrations affect mostly tip and tilt, i.e. the two first coordinates of the modal basis, different types of controllers or different control gains need to be used in order to achieve efficient correction. We shall break the command vector u in two parts and take $u = [u_{\text{tip-tilt}}, u_{\text{HO}}]$, where both components are vectors of lengths respectively 2 and the number of considered higher orders.

Two different controllers will then be tested, depending on the way $u_{\text{tip-tilt}}$ is computed:

5.1 Integrator (INT)

In this case, an integrator is used for all modes. The control voltage is computed as follows:

$$u_k = u_{k-1} + G y_k \tag{1}$$

where u_k and y_k are the command and measurement vectors at time $t = kT_e$, with $T_e = 1/F_e$, where F_e is the AO loop frequency. G is a diagonal gains matrix, with the first two terms equal to $g_{\text{tip-tilt}}$ and the remaining ones to g_{HO} . The results presented in Sect. 5.4 are given with G optimized in order to obtain the highest possible Strehl ratio.

5.2 Mixed LQG/integrator (LQG+INT)

The LQG+INT is a mixed controller where an LQG regulator is used for tip and tilt and an integrator (INT) for the remaining modes.

The tip and tilt control loops are decoupled. Each (scalar) tip or tilt regulator is a predictive controller based on a stochastic model of the total tip or tilt aberrations. This model is taken in the generic state-space form

$$\left\{ \begin{array}{lcl} X_{k+1}^{\mathrm{TT}} & = & A_{\mathrm{TT}} X_k^{\mathrm{TT}} + \Gamma_{\mathrm{TT}} \nu_k^{\mathrm{TT}} \\ \phi_k^{\mathrm{TT}} & = & C_{\mathrm{TT}} X_k^{\mathrm{TT}} \\ \phi_{k-1}^{\mathrm{TT}} & = & C_{\mathrm{TT},2} X_k^{\mathrm{TT}} \end{array} \right. \tag{2}$$

where ν_k^{TT} is a Gaussian zero-mean white noise with covariance matrix $\Sigma_{\nu,\mathrm{TT}}$. This disturbance model is computed from telemetry data, using the subspace identification algorithm N4SID[4] with enforced stability.[5] Once the matrices are identified, their values are refined using Prediction Error Minimization. These identifications are performed under Matlab©. Fig. 2 is an example showing how well the PSD of the identified model fits the PSD of pseudo-open loop data. (The order of the identified model was optimized and taken equal to nOrder = 16.)

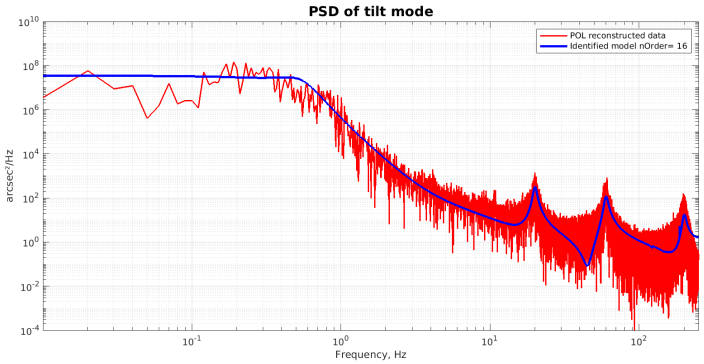

Figure 2. Example of tilt PSD in the scenario **[ATM]+[WIND]+[VIB]** (red curve) with the result of identification superimposed to it (blue curve)

Once the disturbance model is calculated, the next step is to build an asymptotic Kalman filter in order to predict the total incoming disturbance ϕ^{TT} :

$$\left\{ \begin{array}{lcl} \widehat{X}_{k+1|k}^{\mathrm{TT}} & = & (A_{\mathrm{TT}} - L_\infty) \widehat{X}_{k|k-1}^{\mathrm{TT}} + L_\infty (y_k^{\mathrm{TT}} - D\phi_{k-1}^{\mathrm{cor}}) \\ \widehat{\phi}_{k+1|k}^{\mathrm{TT}} & = & C_{\mathrm{TT}} \widehat{X}_{k+1|k}^{\mathrm{TT}} \end{array} \right. \tag{3}$$

where D is the WFS matrix. We consider a standard with a two-frame loop delay. In the case of instantaneous response, we have $\phi_k^{\mathrm{cor}} = u_{k-1}$, we can simply write:

$$\widehat{X}_{\mathrm{k+1|k}}^{\mathrm{TT}} = (A_{\mathrm{TT}} - L_\infty) \widehat{X}_{\mathrm{k|k-1}}^{\mathrm{TT}} + L_\infty (y_k^{\mathrm{TT}} - D u_{k-2}) \tag{4}$$

The Kalman gain L_∞ is computed from A_{TT}, $C_{\mathrm{TT},2}$, $\Sigma_{\nu,\mathrm{TT}}$ and the measurement's noise variance matrix $\Sigma_{\mathrm{w,TT}}$. This calculation centrally requires solving an algebraic Riccati equation.

The LQG controller can be put into state-space form as follows:

$$\left\{ \begin{array}{lcl} X_{k+1}^{\mathrm{LQG}} & = & A_{\mathrm{LQG}} X_k^{\mathrm{LQG}} + B_{\mathrm{LQG}} y_k \\ u_{\mathrm{TT},k}^{\mathrm{LQG}} & = & C_{\mathrm{LQG}} X_{k+1}^{\mathrm{LQG}} \end{array} \right. \tag{5}$$

For the higher order modes, a standard integrator with optimized gain is used.

5.3 Simulations conditions

Simulations are performed using COMPASS simulator.[6] The guide star has a magnitude of 12 (medium flux). The simulations are performed with a total AO loop delay of 2 frames, as mentioned above, and a running frequency $F_e = 500$Hz.

Performance is evaluated by computing the long-exposure Strehl ratio for residual phase trajectories of $N_{perf} = 5000$ points (10 seconds).

5.4 Results

We summarize in Table 1 the performance of both regulators for the given scenarios. Both INT and INT+LQG are tuned to give best performance.

	[ATM]	[ATM]+[WIND]	[ATM]+[WIND]+[VIB]
INT	79%	57%	48%
LQG+INT	79%	77%	71%

Table 1. End-to-end COMPASS results

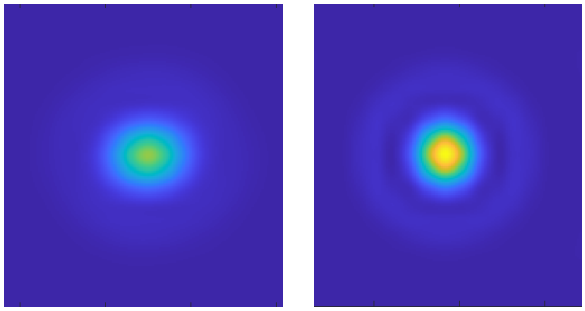

Figure 3. PSF in [ATM]+[WIND]+[VIB] case using INT (left) or LQG+INT (right)

As expected, INT handles poorly disturbances from non atmospheric origin, whereas LQG+INT reaches the performance target in all scenarios. Here we show an example of how each controller compensates scenario 3 disturbances: Fig. 3.

All the previous results were given in the case where all the correction mirrors have instantaneous response. In the next section, we tackle the case where M4 has temporal dynamics.

6. SIMULATIONS WITH M4 DYNAMICS

6.1 M4 dynamics

As noted in the introduction, the MICADO tip and tilt control efforts are split between the M4 and M5 mirrors. M5's response is significantly slower. Because of that, it is expected that the rejection bandwidth of the resulting combination of M4+M5 will be similar to what would be achieved with a stand-alone high-stroke version of M4. In this case, the M4 dynamics would be the main limitation on closed-loop performance.

To evaluate the impact of M4 dynamics, we use the continuous-time model provided by ESO, without the additional delay. The dynamics are assumed to be linear and fully decoupled, with the diagonal (modal) transfer function:

$$TF_{M4}(s) = \frac{1}{1.147\ 10^{-7}s^2 + 4.402\ 10^{-4}s + 1} \tag{6}$$

The associated damping factor and natural frequency are respectively equal to $\xi = 0.65$ and $f_N = 469.9$ Hz.

We show in Fig. 4 the difference between the correction phase ϕ^{cor} without and with M4 dynamics, for a short sequence of scalar controls and a sampling frequency $F_e = 500$ Hz. Note that with M4's dynamics, the correction phase reaches its target value only during the second half of each sampling period.

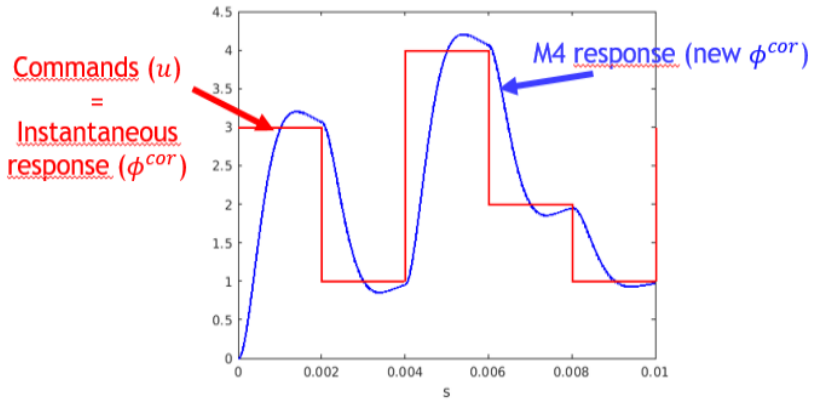

Figure 4. Comparison between the correction phases for a DM with instantaneous response $\phi^{\text{cor}} = u$) and the M4 response considering its dynamics (new ϕ^{cor}), at $F_e = 500$ Hz.

6.2 Performance evaluation: tilt only

In this section, we elaborate a scalar loop by adding M4 dynamics to assess its impact on performance. To do so, we express all the phases, commands and measurements in the same already presented modal basis i.e. we do not deal with transformations from signals/phase screens to modes. Given that, all data are in nm rms and not in Strehl ratio because we omit other error budget terms and the loop is simplified. Also, the variable gain of the pyramid WFS is not taken into account and is considered perfectly linear; it only induces one frame of delay and its gain is 1. We consider the 3 scenarios introduced in Sec. 3.

6.3 Controllers

i) **Integrator** with optimized gain
ii) **LQG+M4**: is an LQG controller taking into account the effects of M4 dynamics in the measurement equation and anticipating them to compute the control.

With DM dynamics, the average correction phase over each sampling period is given by

$$\phi_k^{\text{cor}} = \frac{1}{T_e} \int_{(k-1)T_e}^{kT_e} p(t)dt \tag{7}$$

where $p(t)$ represents the instantaneous position of M4.

In LQG+M4, the controller state X^{LQG} is augmented by additional states corresponding to the discretized version of M4's dynamics. These additional states then enable to compute the correct value of ϕ_{k-1}^{cor} for the Kalman filter. They also enable to compute the value of u_k which ensures that the identity $\phi_{\text{k+1}}^{\text{cor}} = \widehat{\phi}_{k+1|k}$ holds (dead-beat control).

6.4 Results

In Table 2, we recall the root mean square (rms) values of each used sequence. We the give the performance of LQG control (as in Sect. 5.4) when M4 is considered infinitely fast. The corresponding line in Table 2 is the reference we take to compare the controllers.

	[ATM]	[ATM]+[WIND]	[ATM]+[WIND]+[VIB]
σ_{tip} (open loop)	171	1411	1411
Instantaneous response case			
Reference: LQG	38	53	108
M4 dynamics			
INT	43	97	157
LQG+M4	38	49	107

Table 2. Scalar AO loop results with and without M4 dynamics in nm rms

It is obvious that the integrator exceeds reference values in all scenarios and does not have good performance in windshake and vibrations cases. On the other hand, LQG+M4 has much better performance in all scenarios and allows to cancel the effects of M4 dynamics and to recover the same level of performance than for the reference.

7. CONCLUSION

In this paper we showed how standard integrator compensates poorly complex disturbances, and how a model-based LQG control based on tip/tilt models identified from AO telemetry allows to reach targeted performance even when the effect of M4 dynamics is taken into account. In fact we developed a flexible tool allowing to assess the impact of any mirror dynamics on performance, for any disturbance scenario.

Since observational conditions varies over time, we need to re-identify the disturbance models and update the controllers accordingly. This may create transient bumps in the control and residual phase trajectories. Therefore, bumps management is to be considered.

For MICADO SCAO, LQG will be implemented in the Real Time Computer (RTC) as it was validated in the Final Design Review (FDR). We also plan to evaluate the impact of M4 dynamics on all (about 4 000) control modes. In addition, the impact of the split of tip-tilt commands between M4 ad M5 done by ESO at the level of the ELT Central Control System needs to be investigated.

REFERENCES

[1] Davies, R., Alves, J., Clénet, Y., et al., "The final design of MICADO, the first light ELT camera," in [*Ground-based and Airborne Instrumentation for Astronomy IX*], *Proc. SPIE* **this conference** (2022).

[2] Clénet, Y., Buey, T., Gendron, E., et al., "The MICADO first light imager for the ELT: overview of the SCAO module at its final design," in [*Adaptive Optics Systems VIII*], *Proc. SPIE* **this conference** (2022).

[3] Ciliegi, P., Agapito, G., Aliverti, M., et al., "MAORY/MORFEO@ELT: general overview up to the preliminary design and a look towards the final design," in [*Adaptive Optics Systems VIII*], *Proc. SPIE* **this conference** (2022).

[4] Van Overschee, P. and De Moor, B., [*Subspace identification for linear systems: Theory—Implementation—Applications*], Springer Science & Business Media (2012).

[5] Chui, N. L. C. and Maciejowski, J. M., "Realization of stable models with subspace methods," *Automatica* **32**(11), 1587–1595 (1996).

[6] Ferreira, F., Gratadour, D., Sevin, A., et al., "Real-time end-to-end AO simulations at ELT scale on multiple GPUs with the COMPASS platform," in [*Adaptive Optics Systems VI*], *Proc. SPIE* **10703** (2018).